

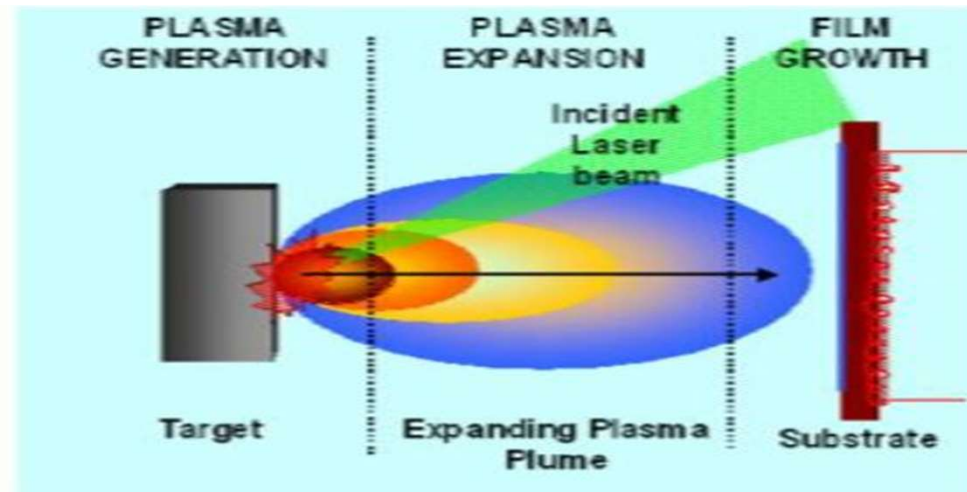


University of Trento  
Physics Department



Antonio Miotello

## DLC and nanometric-sized fluorescent diamonds obtained by laser ablation



International Workshop on  
**Resistive Coatings for Gaseous Detectors**  
Bari- May 13 - 14, 2019

# OUTLINE

- 1) A simple introduction on laser-irradiation of solids;
- 2) Macroscopic models to describe the thermal regime;
- 3) Mechanisms of laser-induced ablation;
- 4) Laser for DLC and nanodiamonds production, with a note on their applications.

## RELEVANT TIME SCALES ON LASER-SURFACE INTERACTION

Energy deposition:  
(it depends on the laser pulse duration) from ns to fs

Electron-electron thermalization:  $10^{-15}$  s

Electron-phonon thermalization:  $10^{-13}$  s

Possible high temperature “liquid-phase”  
duration:  
(it depends on the laser pulse duration) from  $\mu$ s to ps

## THE “MACROSCOPIC ” MODEL TO DESCRIBE THE THERMAL REGIME

$$C_e(T_e) \frac{\partial T_e}{\partial t} = \frac{1}{r} \frac{\partial}{\partial r} \left[ r K_e(T_e) \frac{\partial T_e}{\partial r} \right] - g \cdot (T_e - T_l) + A(r, l),$$

$$C_l(T_l) \frac{\partial T_l}{\partial t} = \frac{1}{r} \frac{\partial}{\partial r} \left[ r K_l(T_l) \frac{\partial T_l}{\partial r} \right] + g \cdot (T_e - T_l) + (Hst)$$

A(r,t): Heat source term, calculated as:

ION IRRADIATION  $\left. \frac{dE}{dr} \right|_{nucl} \rightarrow (Hst) \quad \left. \frac{dE}{dr} \right|_{elect} \quad \text{TABULATED FUNCTIONS}$

LASER IRRADIATION:  $\alpha e^{-\alpha r}$

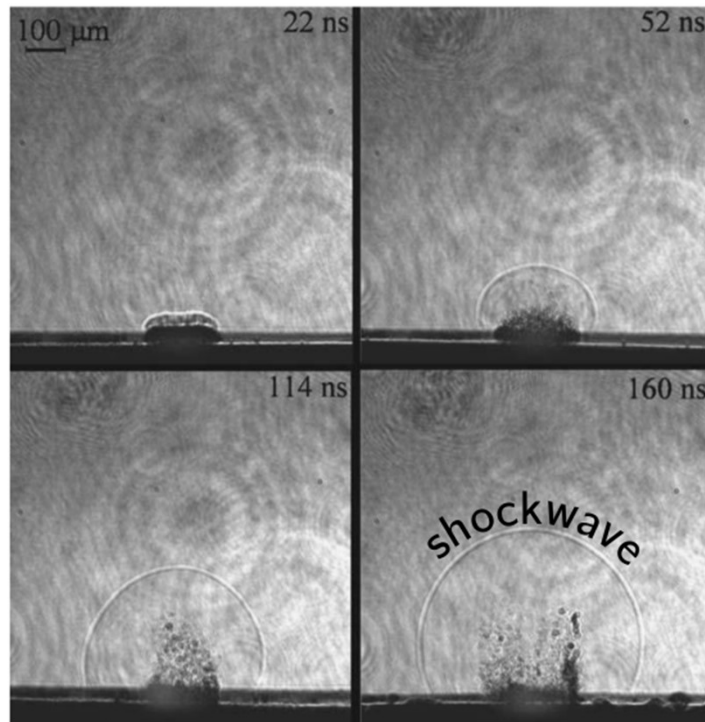
## MECHANISMS OF LASER-INDUCED ABLATION (provided electron-lattice thermalization has occurred)

Different regions form in the target during the ablation process. These regions differ in their expansion dynamics and morphology, and in the thermodynamic relaxation path they follow:

- VAPORIZATION
- SPALLATION
- FRAGMENTATION
- BOILING
- PHASE-EXPLOSION
- SPINODAL DECOMPOSITION

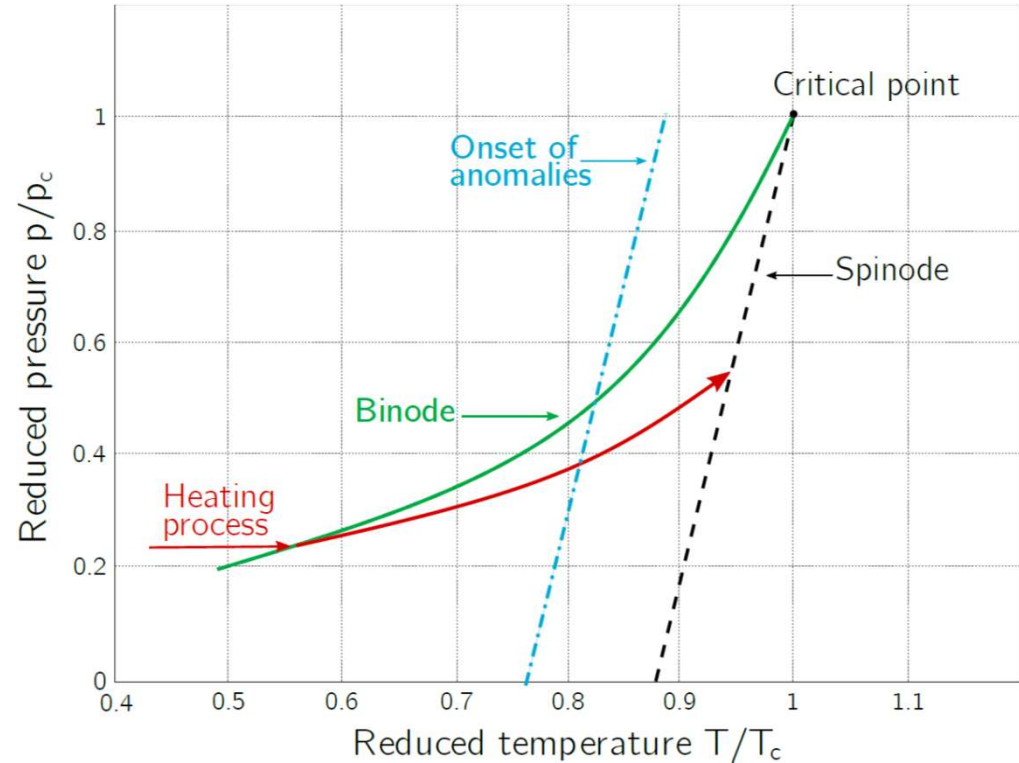
Terminology: *spallation* is sometimes used to describe failure in solids as well as in liquids; we restrict the use of the term to describe the fracture of a solid in which the tensile strength is exceeded. In contrast, the failure of a liquid under tension by nucleation of gas bubbles (while the system is in a metastable state) will be referred to as *cavitation*.

# Mass removal mechanisms through fast vaporization which leads to shock waves with a background gas



PLA of Al, 5 ns pulse,  $5.2 \text{ J/cm}^2$

[C. Porneala and D.A. Willis Appl.Phys.Lett. 89, 211121 (2006)]



# Near surface region

Once that temperature value at the surface ( $T_s$ ) is known, gas-dynamical quantities in the near surface region can be computed:

1. Vapor pressure is obtained by integrating the Clausius-Clapeyron equation, with  $T_b = 2743 \text{ K}$  normal boiling temperature of Al

$$p_{\text{vap}}(T_s) = p_0 \exp \left[ \frac{\Delta H_{\text{vap}}(T_s - T_b)}{RT_s T_b} \right]$$

2. Vapor density is calculated, as a first approximation, from the ideal gas law

$$n_{\text{vap}}(T_s) = \frac{P_{\text{vap}}(T_s)}{k_B T_s}$$

# NORMAL VAPORIZATION

Table 1

Atom layers ( $\lambda$ ) removed by normal vaporization at temperatures straddling  $T_b$  for various substances listed in order of  $T_m$ . Unless otherwise indicated we give information in each case appropriate to  $\text{metal}(\ell) \rightarrow \text{metal}(g)$ , where  $\ell$  refers to liquid and  $g$  refers to gas. The evaluations were made with Eq. (2c), into which vapor pressures ( $p_{atm}^{sv}$ ) from [24-27] were introduced.

Substance	$T$ (K)	Atom layers in 1 ns	Atom layers in 100 ns	$T_b$ (K)	$T$ (K)	Atom layers in 1 ns	Atom layers in 100 ns
Na	1000	0.020	2.0	1156	1500	0.78	78
Bi <sup>(a)</sup>	1000	0.000	0.000	1837	2000	0.058	5.80
Sb <sup>(b)</sup>	1000	0.000	0.002	1860	2000	0.047	4.7
Ag	2000	0.002	0.24	2435	3000	0.31	30.5
U	4000	0.005	0.48	4404	5000	0.069	6.9
Nb	4500	0.003	0.27	5017	5500	0.069	6.9
Mo	4000	0.001	0.092	4912	5000	0.028	2.8
W	5000	0.000	0.041	5828	6000	0.010	1.04

<sup>(a)</sup>The sum of two processes, involving Bi( $g$ ) and Bi<sub>2</sub>( $g$ ), was considered.

<sup>(b)</sup>The sum of three processes, involving Sb( $g$ ), Sb<sub>2</sub>( $g$ ), and Sb<sub>4</sub>( $g$ ), was considered.

$$\text{flux} = \alpha(p_v - p_a)(2\pi m k_B T_s)^{-1/2} \text{ particles cm}^{-2}\text{s}^{-1}$$

$$\left( \frac{dX}{dt} \right) \Big|_{x=0} = \alpha p_{sv} (2\pi m k_B T)^{-1/2} \lambda^3$$

# The Knudsen layer

- The evaporation of the solid/liquid surface is releasing atoms/molecules in the half space above it, **at random angles with respect to the normal of the surface with the velocities following a *half*-Maxwellian distribution at the temperature of the surface  $T_s$ .**
- If the **flux of evaporated particles is dense enough, they collide with each other that results in the development of equilibrium (full Maxwellian distribution) in the particle flow.** The process of establishing the equilibrium occurs within a region, very near to the surface (after only a few mean free paths of emitted atoms/molecules), that is known as the **Knudsen layer (KL)** where the vaporized particles, initially having only positive velocities directed off the surface, develop negative velocities (back to the surface).
- As the particles **momentum is conserved, the particle flow develops a positive center-of-mass (or flow) velocity. The velocity distribution function of atom/molecules at the boundary of the Knudsen layer finally takes the form of a shifted Maxwellian.** The vapor parameters (temperature, pressure, and density) undergo jumps across this layer that is important for adequate gasdynamic simulations of the laser ablation plume expansion.

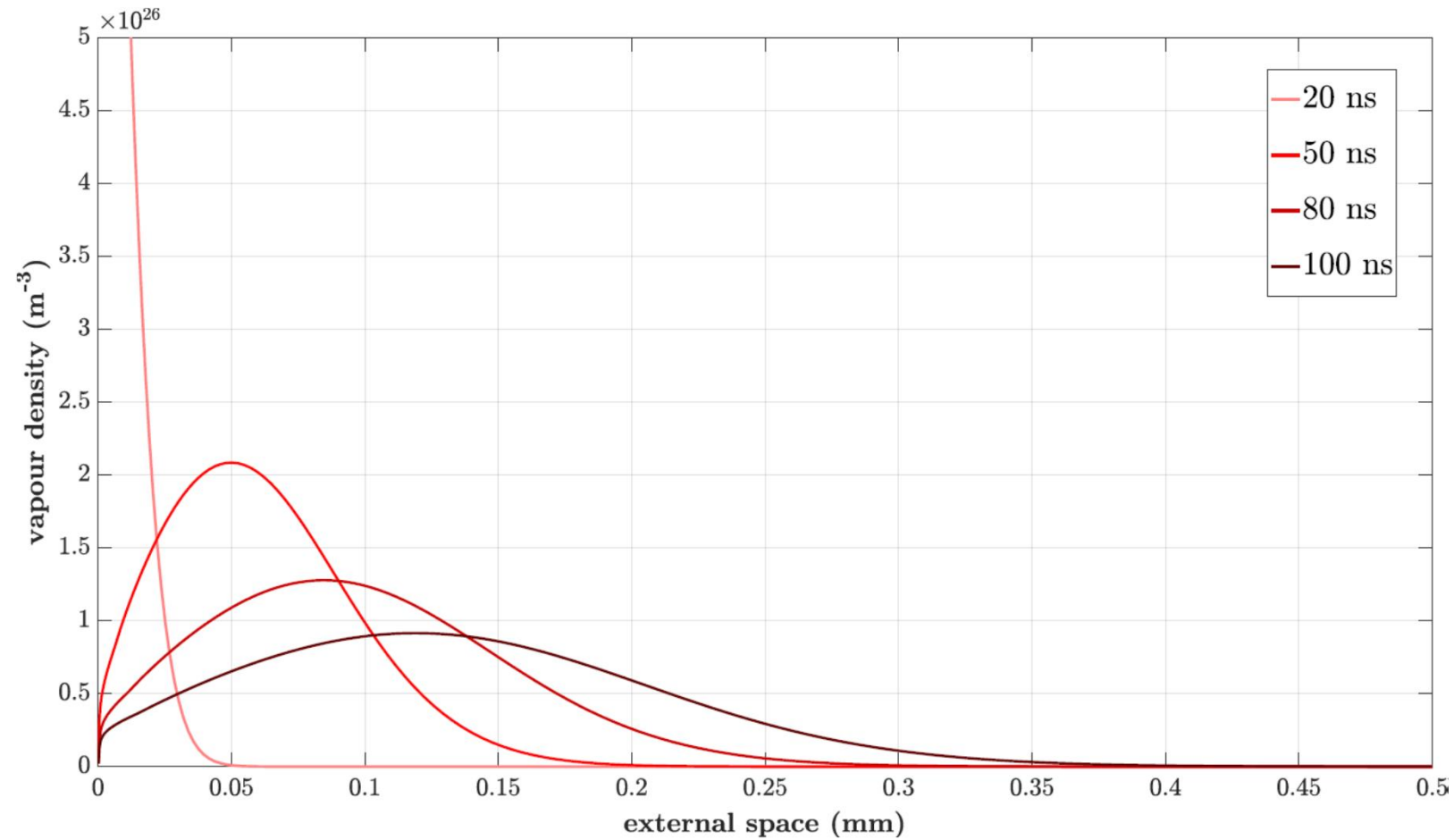
# External vacuum

The vapor plume expansion is described by the Euler equation for non-viscous compressible media

$$\left\{ \begin{array}{l} \frac{\partial \rho}{\partial t} = -\frac{\partial(\rho v)}{\partial x} \\ \frac{\partial(\rho v)}{\partial t} = -\frac{\partial}{\partial x} (p + \rho v^2) \\ \frac{\partial}{\partial t} \rho \left( E + \frac{v^2}{2} \right) = -\frac{\partial}{\partial x} \rho v \left( E + \frac{p}{\rho} + \frac{v^2}{2} \right) \end{array} \right.$$

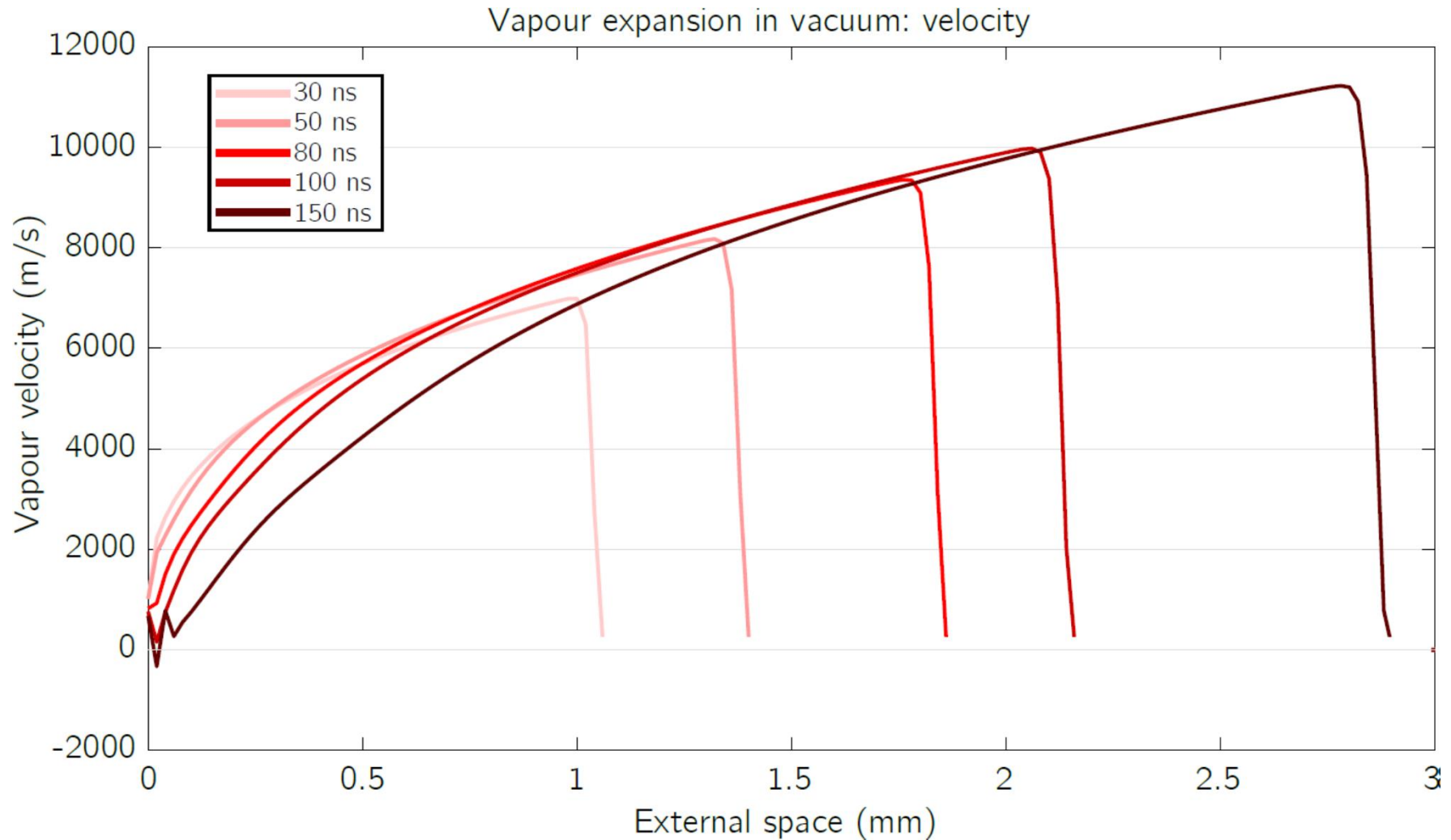
# Simulation results

(laser pulse: 20 ns,  $\lambda=248$  nm,  $3.0 \text{ Jcm}^{-2}$ , Al target)

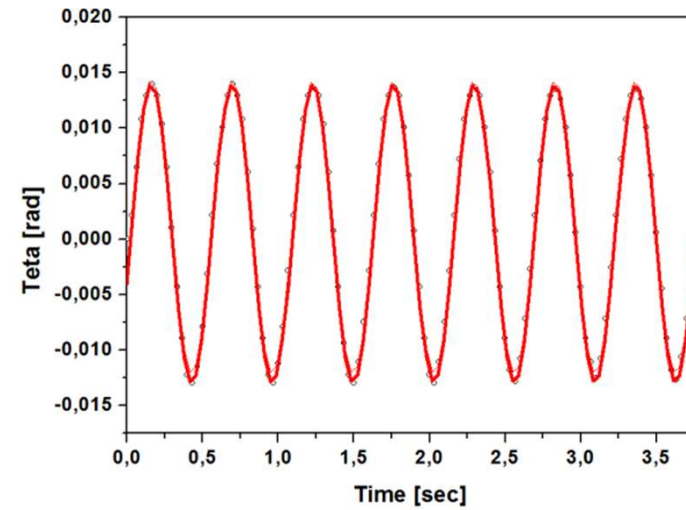
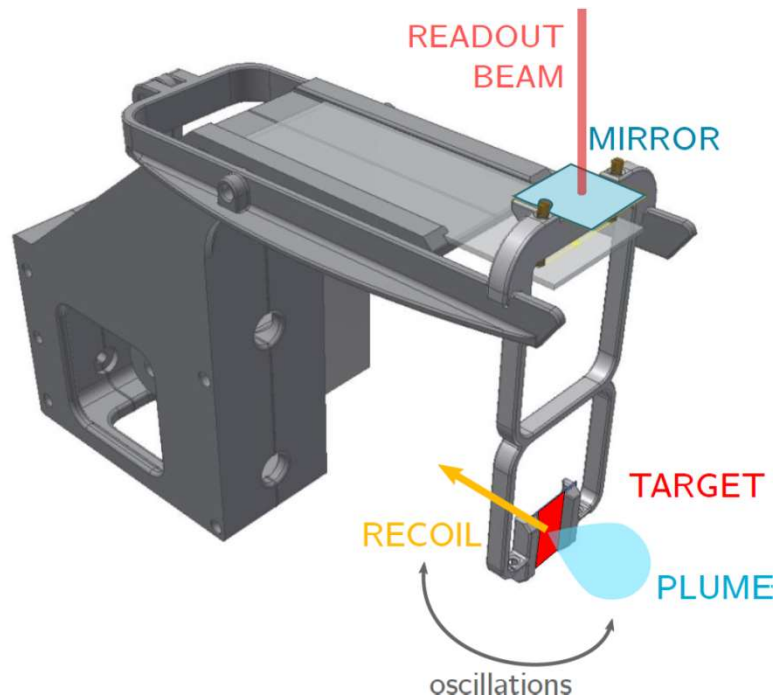


# Simulation results

(laser pulse: 20 ns,  $\lambda=248$  nm,  $3.0 \text{ Jcm}^{-2}$ , Al target)



# Comparison with experimental results



Ballistic pendulum: the oscillation period provides the actual momentum of inertia

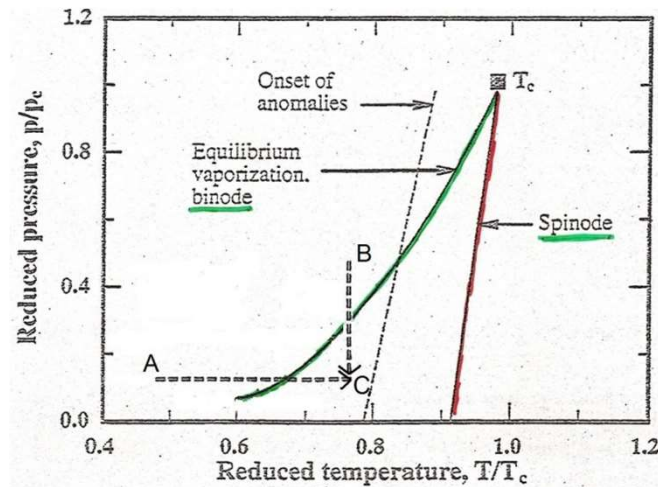


Fig. 1.  $P-T$  diagram near the critical point.

Heating curves (AC,BC) adapted from V.P. Skripov  
"Metastable Liquids" (Halsted Press, New York, 1974)

### BOILING TEMPERATURE

liquid and vapor phases are in equilibrium → see binode line — calculated from the Clausius-Clapeyron equation

**UNDER RAPID HEATING IT IS POSSIBLE TO SUPERHEAT THE LIQUID ABOVE THE BOILING POINT:**

however there is a well defined upper limit for the superheating of a liquid, the spinode

**THE SPINODE IS DETERMINED BY:**

$$\left(\frac{\partial P}{\partial V}\right)_T = 0; \quad \left(\frac{\partial T}{\partial S}\right)_P = 0$$

Using the previous equations and the Berthelot equation the spinode function may be derived

**REMEMBER:**

$$\left(\frac{\partial P}{\partial V}\right)_T = -\frac{k_B T}{(\Delta V)^2} \quad \text{and} \quad \left(\frac{\partial T}{\partial S}\right)_P = \frac{k_B T^3}{(\Delta H)^2}$$

# PHASE EXPLOSION

## REMEMBER:

normal boiling involves heterogeneous nucleation  
at a temperature only minimally higher than  $T_b$

## IF SUPERHEATING OCCURS

and the temperature lies sufficiently near  $T_{tc}$  phase explosion occurs by homogeneous nucleation: the hot region breaks down into vapor plus liquid droplets

## RATE OF HOMOGENEOUS NUCLEATION:

$$I_n \approx 1.5 \times 10^{32} \exp \left( \Delta G_n / k_B T \right) \times \exp \left( - \tau_{hn} / t \right)$$

$\Delta G_n$  = free energy for formation of a stable homogeneous nucleus

$\tau_{hn}$  = time constant of the process (in the range from ns to ps)

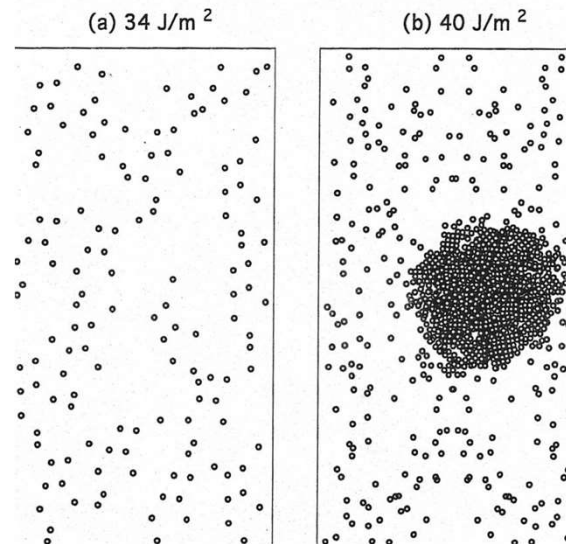
## The Cs example:

$$\left. \begin{array}{l} I_n = 1 \text{ cm}^{-3} \text{ s}^{-1} \quad \text{at } T = 0.874 T_{tc} \\ I_n = 10^{26} \text{ cm}^{-3} \text{ s}^{-1} \quad \text{at } T = 0.905 T_{tc} \end{array} \right\}$$

as given by Martynyuk  
J. Phys. Chem. 57  
p. 494 (1983)

**SNAPSHOTS OF THE  
PLUME FROM THE  
MOLECULAR  
DYNAMICS  
SIMULATION**

**AT 400 ps AFTER  
IRRADIATION WITH  
150 ps LASER PULSE**



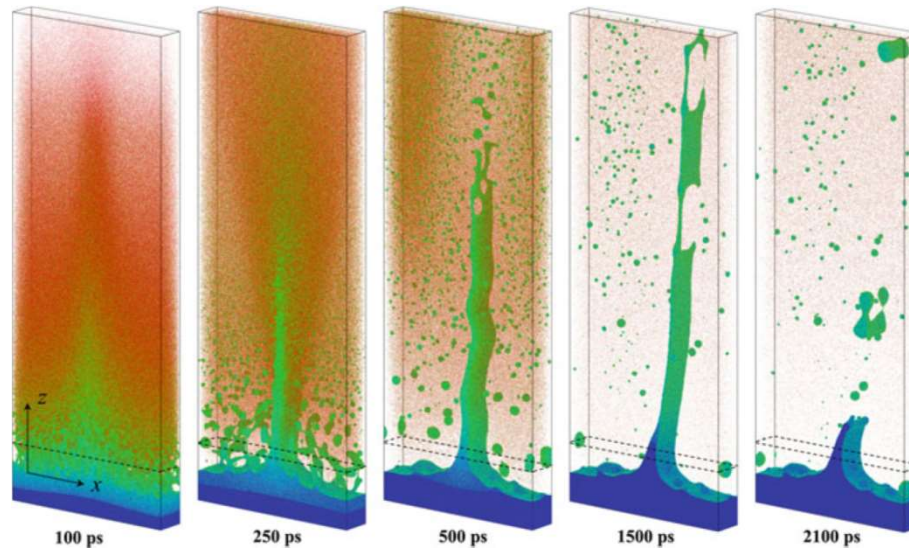
**L.V.ZHIGILEI  
B.J.GARRISON  
Appl.Phys.Lett.  
74 (1999)1341**

**TWO DISTINCT REGIMES OF MOLECULAR EJECTION SEPARATED  
BY A WELL-DEFINED THRESHOLD FLUENCE ARE OBSERVED IN  
MOLECULAR DYNAMICS SIMULATION OF PULSED LASER  
IRRADIATION OF AN ORGANIC SOLID**

- Below threshold thermal desorption from the surface is observed and the desorption yield has an Arrhenius-type dependence on the laser fluence
- Above the threshold a collective multilayer ejection occurs where large liquid droplets are ejected and the total yield of the ablated material follows a critical volume density of the deposited energy

# Modelling laser ablation on metals

L.V. Zhigilei (Virginia University)



## Molecular Dynamics

A sequence of atomistic snapshots generated in a TTM-MD simulation of single pulse ablative LIPSS formation on a Cr surface. **Dark-blue** regions correspond to the solid phase, **light-blue** and **green** represent liquid phase and free surfaces, and **red** atoms belong to the vapor phase.

# Dynamic vapor bubble nucleation

## Vapor bubble growth in superheated liquid metal

$$\begin{cases} R \frac{d^2 R}{dt^2} + \frac{3}{2} \left( \frac{dR}{dt} \right)^2 = \frac{P_v(T) - P_\infty}{\epsilon \rho_l} - \frac{2\sigma(T)}{\epsilon \rho_l R} - 4 \frac{\mu}{\epsilon \rho_l R} \frac{dR}{dt} \\ \frac{\partial T}{\partial t} + u_r \frac{\partial T}{\partial r} = \alpha \left( \frac{\partial^2 T}{\partial r^2} + \frac{2}{r} \frac{\partial T}{\partial r} \right) \end{cases}$$

Thermodynamic-hydrodynamic problem  
numerically solved by [Lee and Merte](#)

Now applied to liquid metals

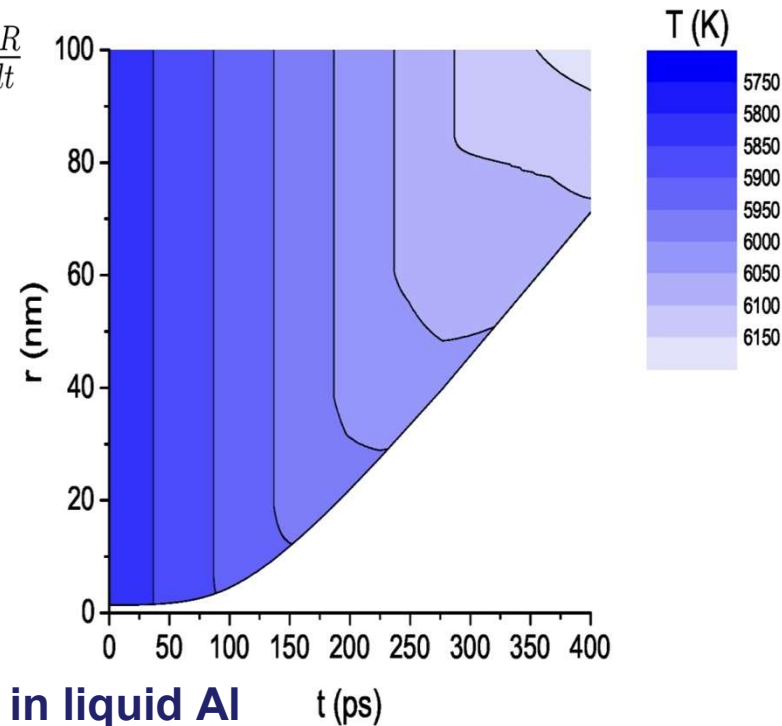


**Figure: single vapor bubble expansion in liquid Al**  $t$  (ps)

# Metastable liquid metals: thermodynamic models

Thermodynamics of metals at  $T > 5000\text{K}$ :  
quantities measured up to  $T_b$

- Theory of critical exponents
- Semiempirical scaling laws based on low  $T_b$  substances

Watson formula for

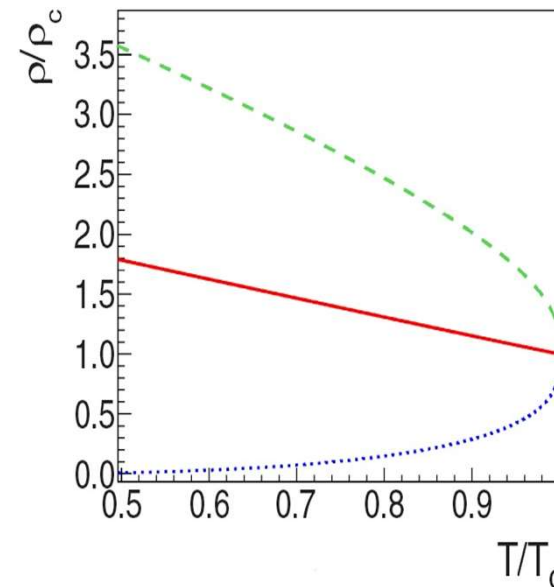
$$\Delta h_v(T) = \Delta h_v(T_b) [(T_c - T)/(T_c - T_b)]^{0.38}$$

K. M. Watson, *Ind. Eng. Chem.* **35**, 398 (1943).

Guggenheim formula for

$$\sigma(T) = \sigma_m [(T_c - T)/(T_c - T_m)]^{11/9}$$

E. A. Guggenheim, *J. Chem. Phys.* **13**, 253 (1945)



Coexistence curve of Fe:  $\rho_l$ ,  $\rho_v$ ,  
 $\rho_d = \frac{1}{2}(\rho_l + \rho_v)$

Degree of coexistence curve:

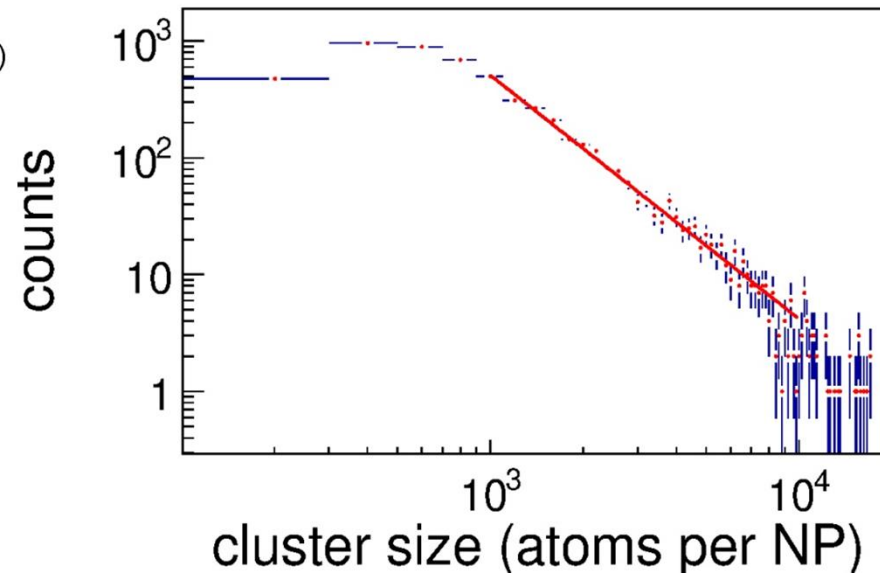
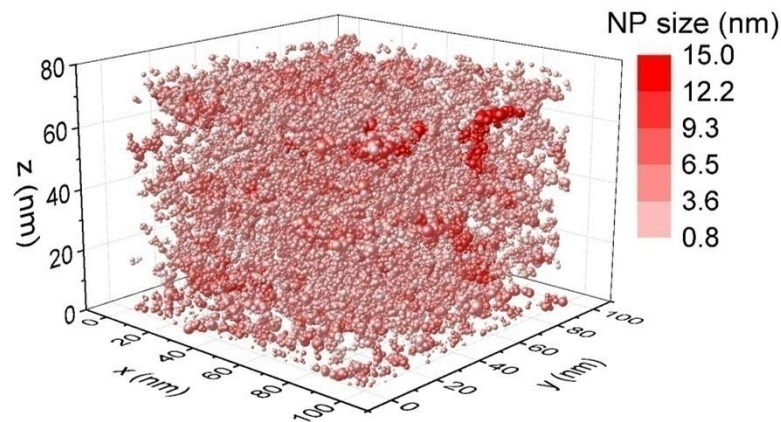
$$\rho_l - \rho_v = \rho_c A_\beta (-\varepsilon)^\beta$$

$\beta$  critical exponent,  $\varepsilon = (T - T_c)/T_c$

# Nanoparticles size distribution: theory

- The thermal phenomena occurring at the target surface are studied within the framework of a thermodynamic continuum approach. A 20 ns laser pulse of variable fluence and gaussian time dependence was assumed. The temperature role in the target external layers is studied through the heat diffusion equation.
- The vaporization from the surface is modeled assuming unsteady adiabatic expansion (UAE) of the vapor and a Monte Carlo (MC) method is used to describe the formation of liquid nanodroplets through phase explosion.

$$F(N) \propto N^{-a} \quad (a=1.9 \pm 0.02) \quad N = \text{atoms per NP}$$



# NPs size distribution: experiments

- Direct TEM observation of narrow size distribution of nanometric Ag NPs
- Consistent with the typical size of vapor bubbles/nanodroplets of our simulations

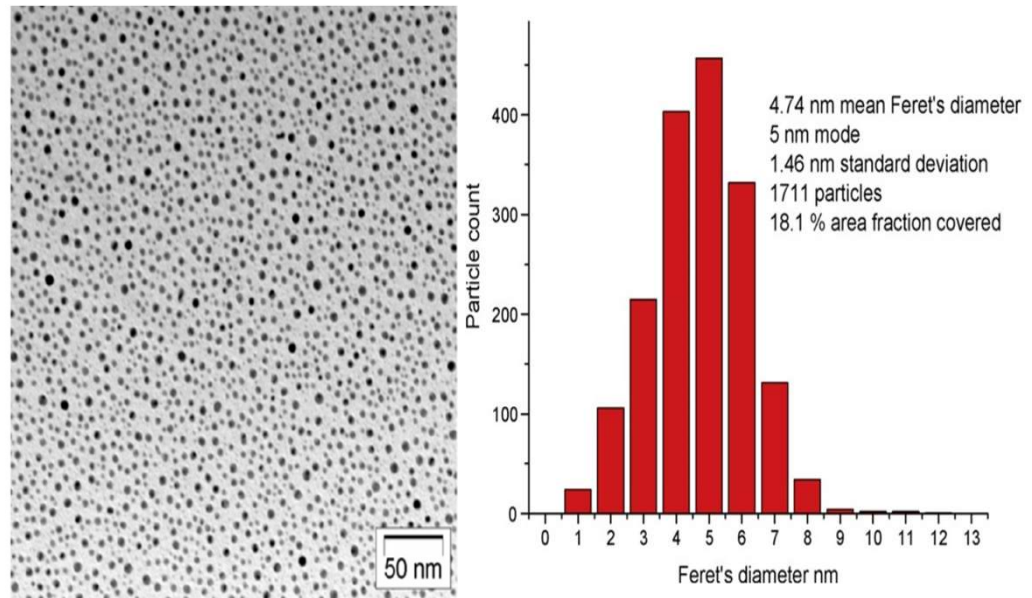
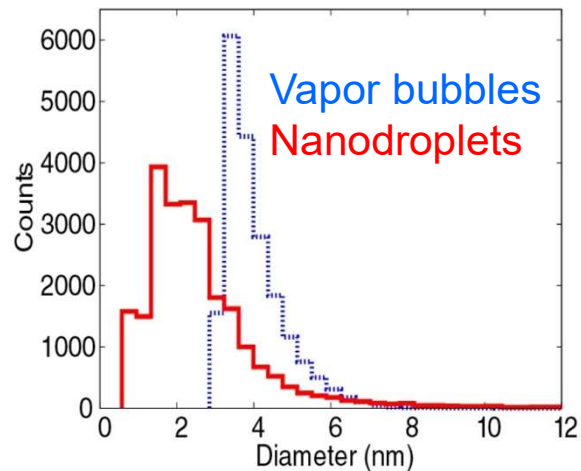
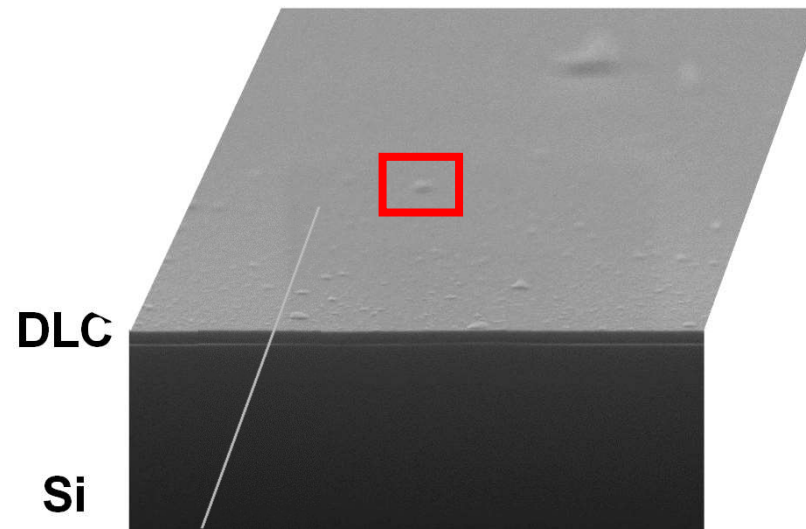
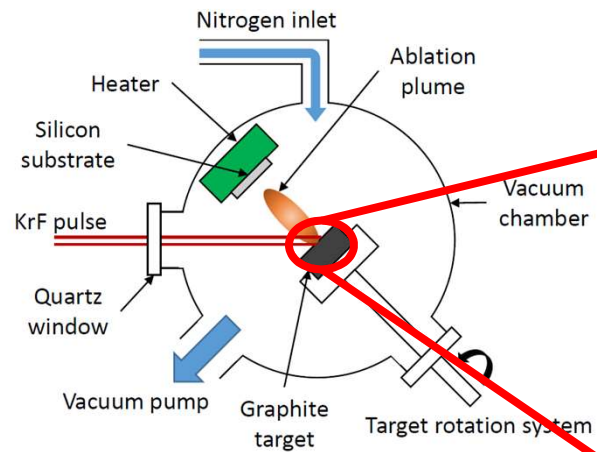


**Figure:** TEM image and size histogram of as-grown films of Ag nanoparticles deposited in vacuum by 500 laser pulses  
Laser: 10 ns; Target: pure Ag

# Production technique of DLC and NDs

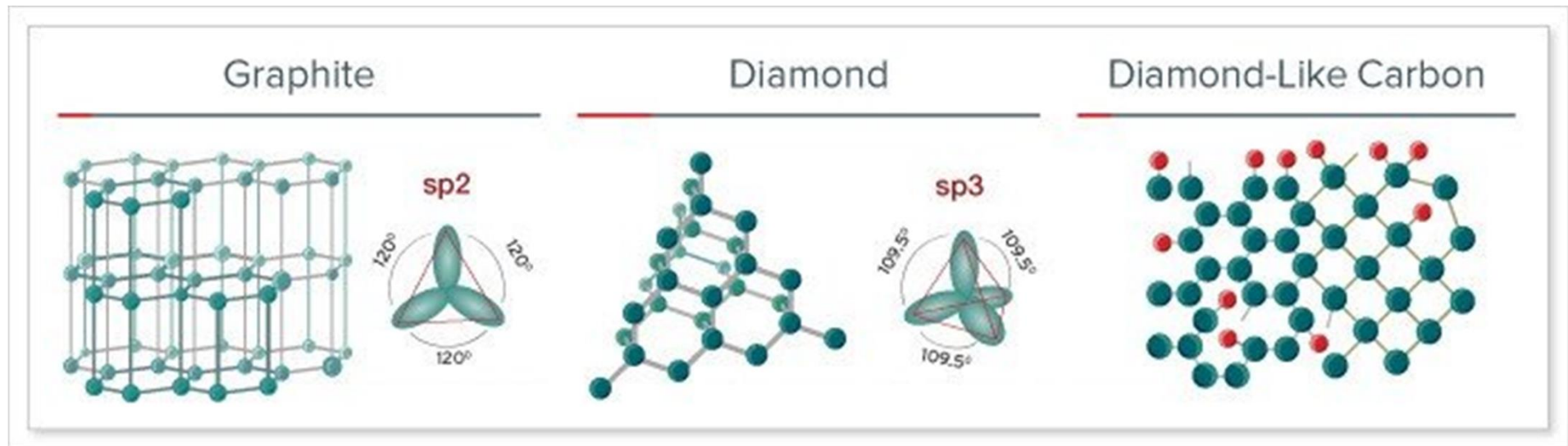
Pulsed laser ablation ( $\lambda=248$  nm, 20 ns,  $7$  J cm<sup>-2</sup>) of a **graphite** target in a controlled **nitrogen** atmosphere



## CARBON FILMS: Physical properties depending on the ratio of $sp^2$ (graphite-like) to $sp^3$ (diamond-like) bonds.

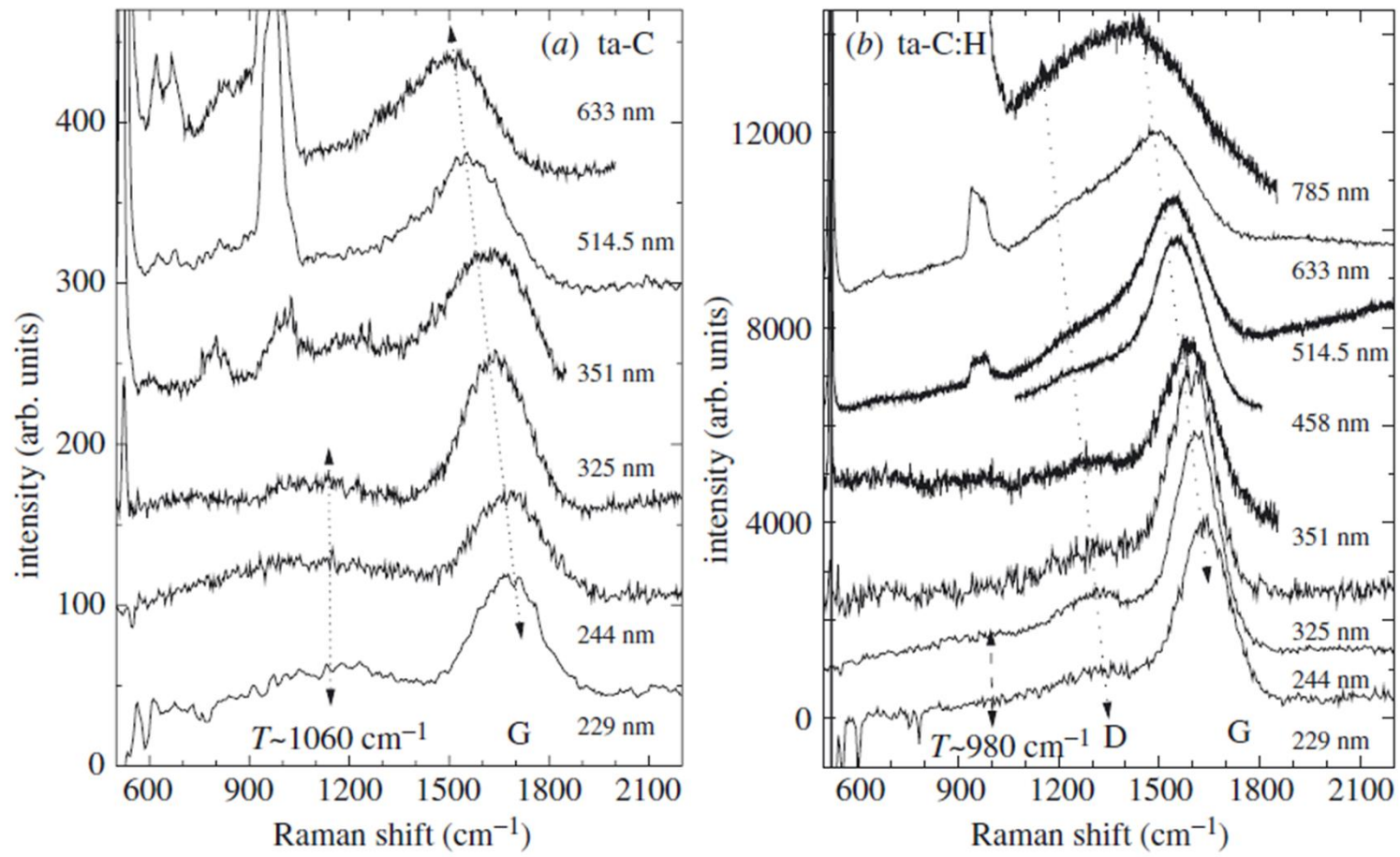
DLCs with highest  $sp^3$  content (80–90%) are called tetrahedral amorphous carbon (ta-C) and the hydrogenated analogue ta-C:H.

In general, an amorphous carbon can have any mixture of  $sp^3$ ,  $sp^2$  and even  $sp^1$  sites, with the possible presence of hydrogen and nitrogen.



**Raman spectroscopy:** Very popular, non-destructive tool for structural characterization of carbon films. All carbons show common features in their Raman spectra in the 800–2000  $\text{cm}^{-1}$  region: the G and D peaks, which lie at ca. 1560 and 1360  $\text{cm}^{-1}$ , respectively, for visible excitation, and the T peak at ca. 1060  $\text{cm}^{-1}$ , seen only in ultraviolet (UV) excitation. The T peak is due to the C–C  $\text{sp}^3$  vibrations.

Details from: A.C. Ferrari and J. Robertson *Phil. Trans. R. Soc. Lond. A* 2004 362, 2477-2512



# DLC films obtained with pulsed (20 ns wavelength of 248 nm) laser deposition, ablating highly oriented pyrolytic graphite at room temperature, in a $10^{-2}$ Pa vacuum, at fluences ranging between 0.5 and 35 J/cm<sup>2</sup>

M.Bonelli, A.C. Ferrari, A. Fioravanti , A.M. et al.: Eur. Phys. J. B 25, 269–280 (2002)

## Film structure was investigated by:

- Raman spectroscopy at different excitation wavelength from 633 nm to 229 nm and Transmission Electron Energy Loss Spectroscopy.
- X-ray reflectivity: roughness, density and cross-sectional layering of selected samples were studied.
- By scratch test film adhesion and friction coefficients between 0.06 and 0.11 were measured. By profilometry we obtained residual stress values not higher than 2 GPa in as-deposited 80% *sp*<sup>3</sup> ta-C films.

Film hardness as high as 70 GPa was obtained by nanoindentation on films deposited with the SiC interlayer.

- The films, which are hydrogen-free, as shown by Fourier Transform Infrared Spectroscopy, undergo a transition from mainly disordered graphitic to up to 80% tetrahedral amorphous carbon (ta-C) **above a threshold laser fluence of 5 J cm<sup>-2</sup>.**

**Why a threshold ?**

**The existence of a threshold fluence at which the film structure changes from graphitic to diamond-like can be traced to a corresponding threshold in the values of ablated particle energy**

**C+ energy exceeding ~100 eV is usually considered a necessary condition to obtain a high  $sp^3/sp^2$  bond ratio**

### **ON THE CONTRARY**

**The growing C film will be graphitic if only neutral, low energy carbon atoms arrive on the substrate.**

**The detected species in the plume produced by laser irradiation of graphite mainly consist of C, C<sub>2</sub>, C<sup>+</sup> and C<sup>++</sup>, where the C<sub>2</sub> component is most probably produced through ion-atom collisions followed by charge neutralisation in the plume.**

## Energetic in the ablation plume created by ultraviolet laser irradiation of various target materials

(B. Angleraud, J. Aubreton, and A. Catherinot: Eur. Phys. J. AP 5, 303-310 (1999))

**Table 2.** Velocity  $V$  (km/s) and kinetic energy  $E_c$  (eV) of the front *versus* laser fluence and background gas pressure. For the calculation of  $E_c$ , only atomic species are taken into account.

$5 \times 10^{-3}$ Pa		B, N	C	Al	Mo	YBC
$7 \text{ J/cm}^2$	$V$	40	44	31	15	15
	$E_c$	91	120	134	110	113
$30 \text{ J/cm}^2$	$V$	52	53	36	21	21
	$E_c$	175	175	182	220	222
$200 \text{ J/cm}^2$	$V$	88	88	60	28	29
	$E_c$	500	440	500	390	420
10 Pa						
$7 \text{ J/cm}^2$	$V$	30	30	22	14	14
	$E_c$	58	56	68	98	99
$30 \text{ J/cm}^2$	$V$	36	32	29	19	20
	$E_c$	84	64	118	180	200
$200 \text{ J/cm}^2$	$V$	60	55	45	23	23
	$E_c$	233	190	280	263	266
500 Pa						
$7 \text{ J/cm}^2$	$V$	6.4	-	-	-	-
	$E_c$	2.7	-	-	-	-

(mean error on the velocity: 10%; on the kinetic energy: 20%)

# ROLE OF AMBIENT PRESSURE IN MORPHOLOGY OF DEPOSITED C-FILMS

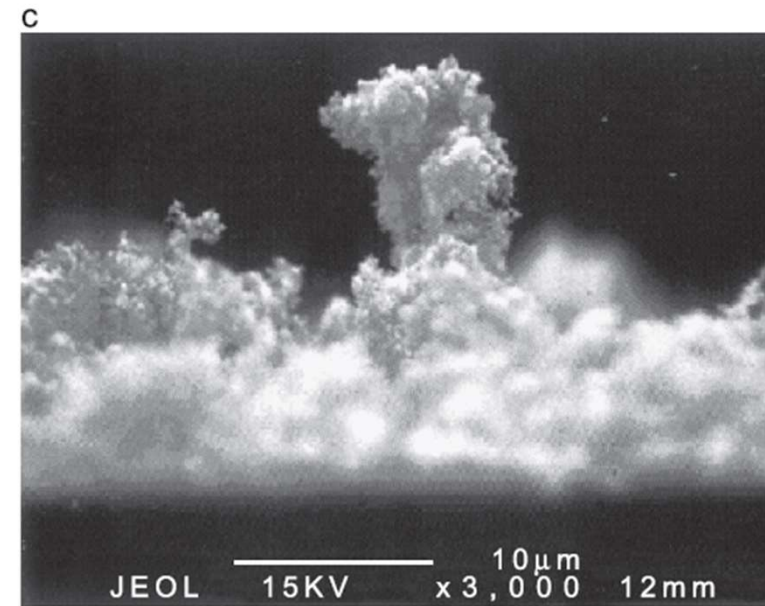
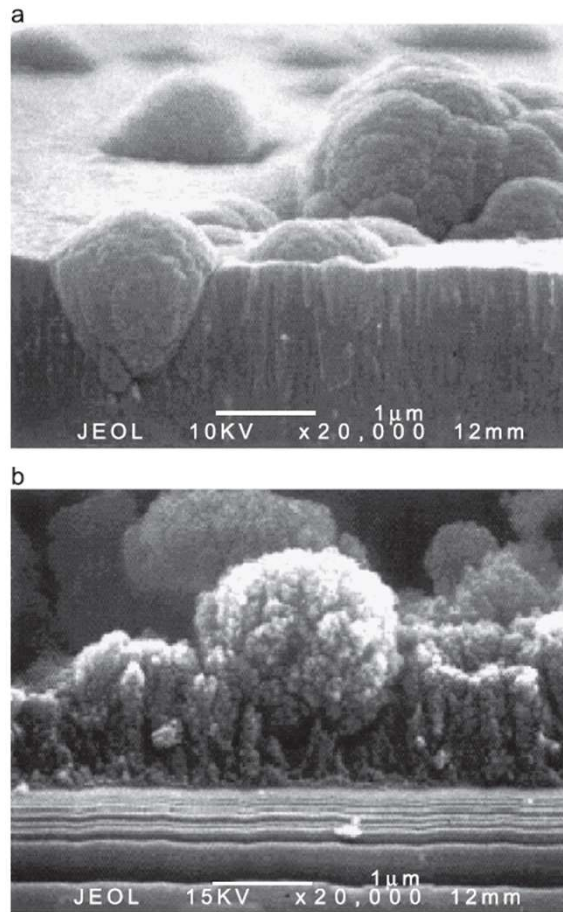


Fig. 5. Cross-sectional SEM micrographs of selected CA films deposited in He atmosphere. (a)  $p_{\text{He}}=50$  Pa,  $P=12.5$  MW mm<sup>-2</sup>; (b)  $p_{\text{He}}=250$  Pa,  $P=8.5$  MW mm<sup>-2</sup>; (c)  $p_{\text{He}}=1$  kPa,  $P=8.5$  MW mm<sup>-2</sup>.

## Pulsed laser deposition of diamond-like carbon films: reducing internal stress by thermal annealing

Paolo Mosaner\*, Marco Bonelli, Antonio Miotello

The Griffith's law:

$$\frac{\sigma_f^2 h_f}{2E_f} \leq 2\gamma \quad (1)$$

establishes a relation between  $\sigma_f$ , the compressive stress in the film, closely related to the elastic energy stored into the film, and  $\gamma$ , the energy per unit area necessary to break the interface: the failure occurs when the left side of Eq. (1) equals the right side. Here,  $h_f$  and  $E_f$  are thickness and elastic modulus of the film, respectively.

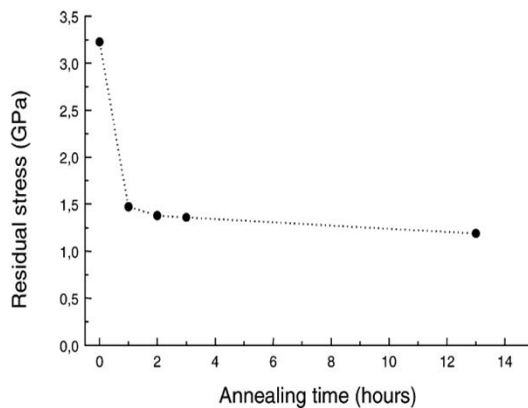


Fig. 4. Compressive stress after several annealing steps. The curve refers to a 375 nm thick film, obtained with a laser energy density of about 40 J/cm<sup>2</sup>.

For thin films, a simplified relation can be used to calculate the stress in the film; this relationship is known as Stoney's equation which reads:

$$\sigma_f = \frac{E_s h_s^2}{6R(1 - \nu_s)h_f} \quad (2)$$

where  $E_s$ ,  $h_s$ , and  $\nu_s$  are respectively elastic modulus, thickness, and Poisson's ratio of the substrate and  $R$  is the curvature radius of the surface.

By evaluating  $\sigma_f$  from Eq. (2), starting from one series of experimental  $h_f$  values, it is possible to study, by looking at Eq. (1), how the critical condition is attained as a function of the film thickness. Nevertheless, it is necessary to establish  $R$  as function of  $h_f$ : this evaluation will be performed by looking at measurements of films having different thickness.

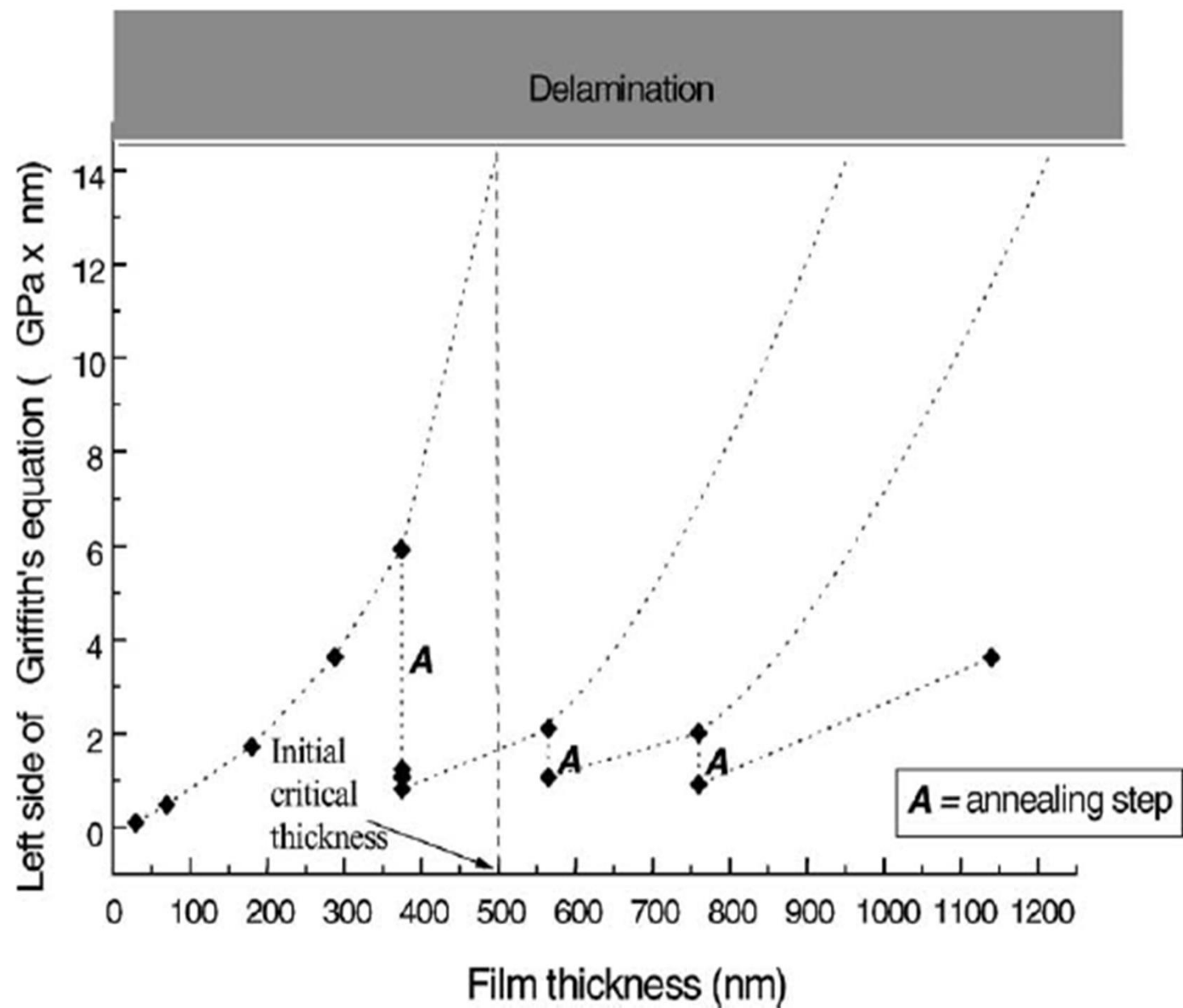
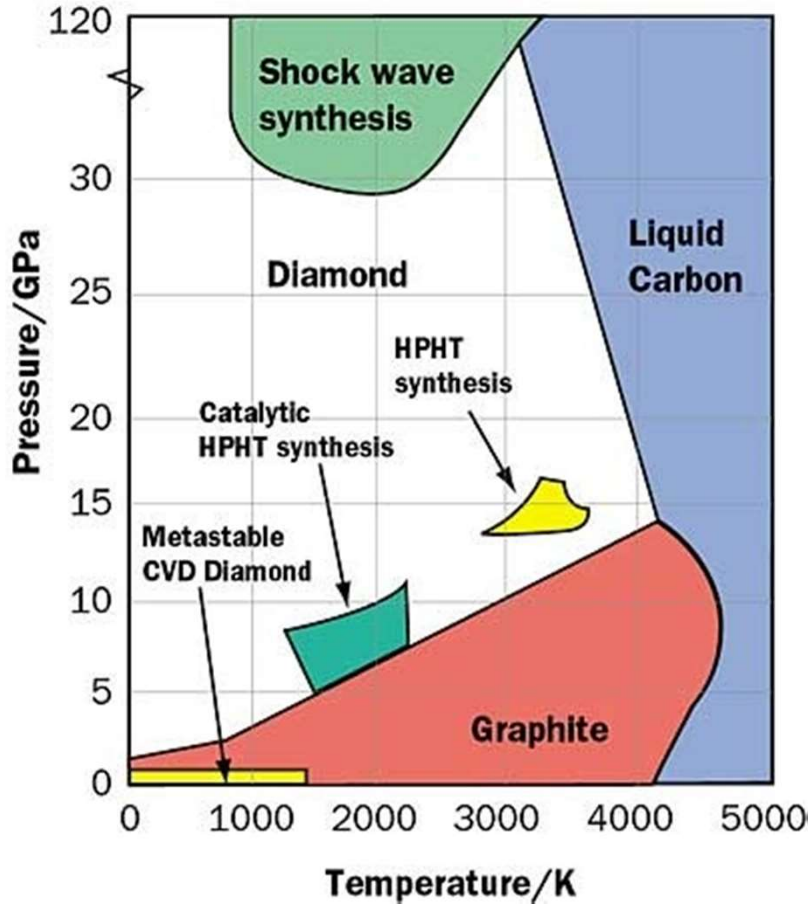


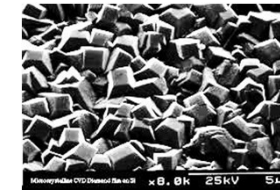
Fig. 5. Compressive stress, as a function of film thickness, after several deposition–annealing steps.

# NANODIAMONDS PRODUCTION

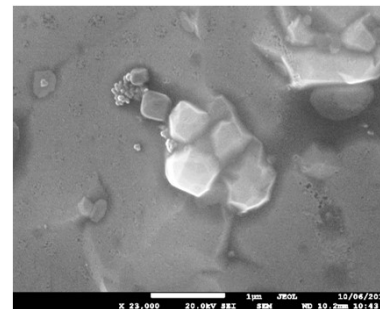
High pressures are required



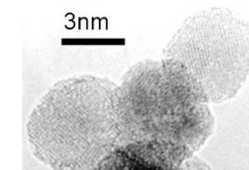
High-pressure-high-temperature (HPHT) diamonds



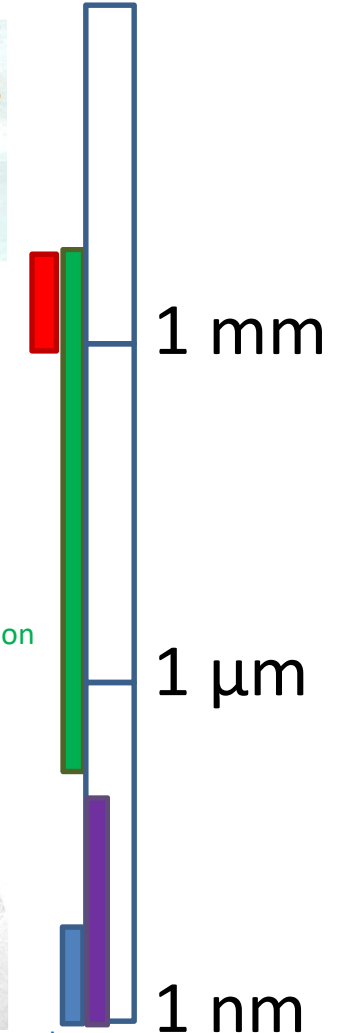
Chemical vapor deposition (CVD) diamonds



Pulsed laser ablation (PLA)

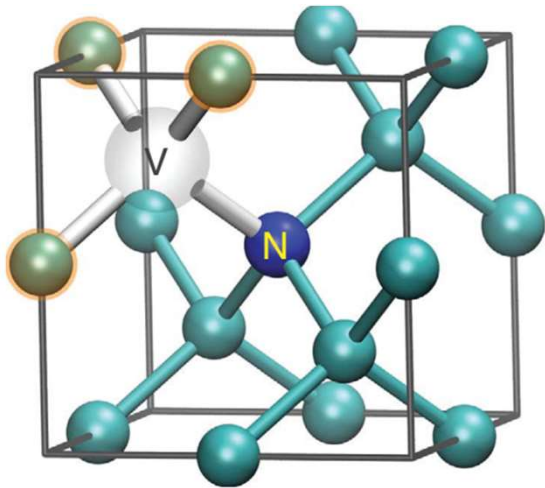


Detonation nanodiamonds



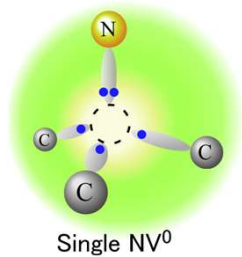
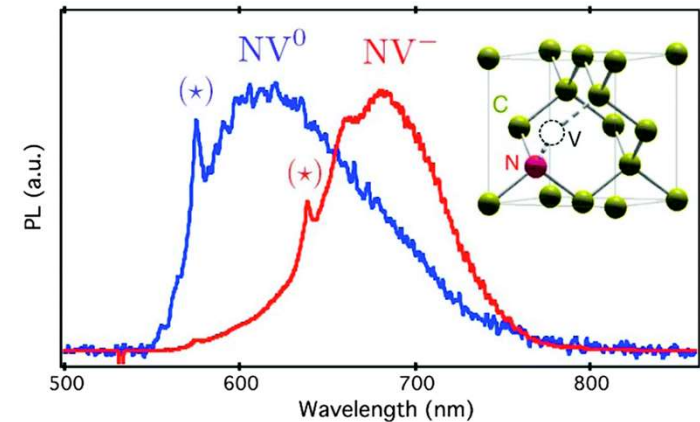
# NV center in diamond

- ❑ Color defect center in diamond (one of the 120 defects!)
- ❑ Paramagnetic
- ❑ High sensitivity to external environment and high spatial resolution
- ❑ NV centers can exist in two charge state:



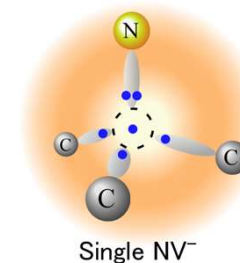
## Applications of NV centers:

- Nanomagnetometry, nanoelectrometry and nanothermometry
- Detection of strain fields
- Confocal and fluorescent bioimaging
- Spin polarization and NMR signal enhancement
- Quantum optics (proposed as solid-state qubit)



**NV<sup>0</sup> ( 5 electrons)**

+1 unpaired  
electron,  $S=+1/2$



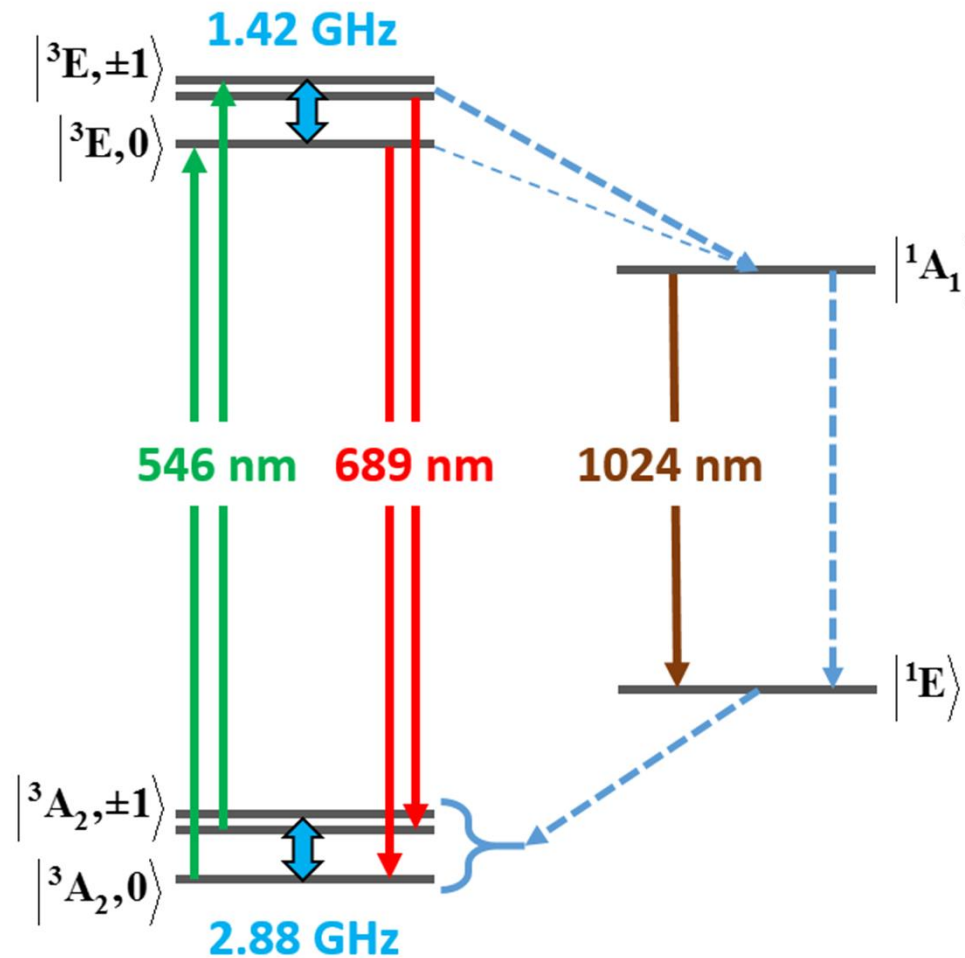
**NV<sup>-</sup> (6 electrons)**

+2 electrons forming  
 $S=+1$  pair

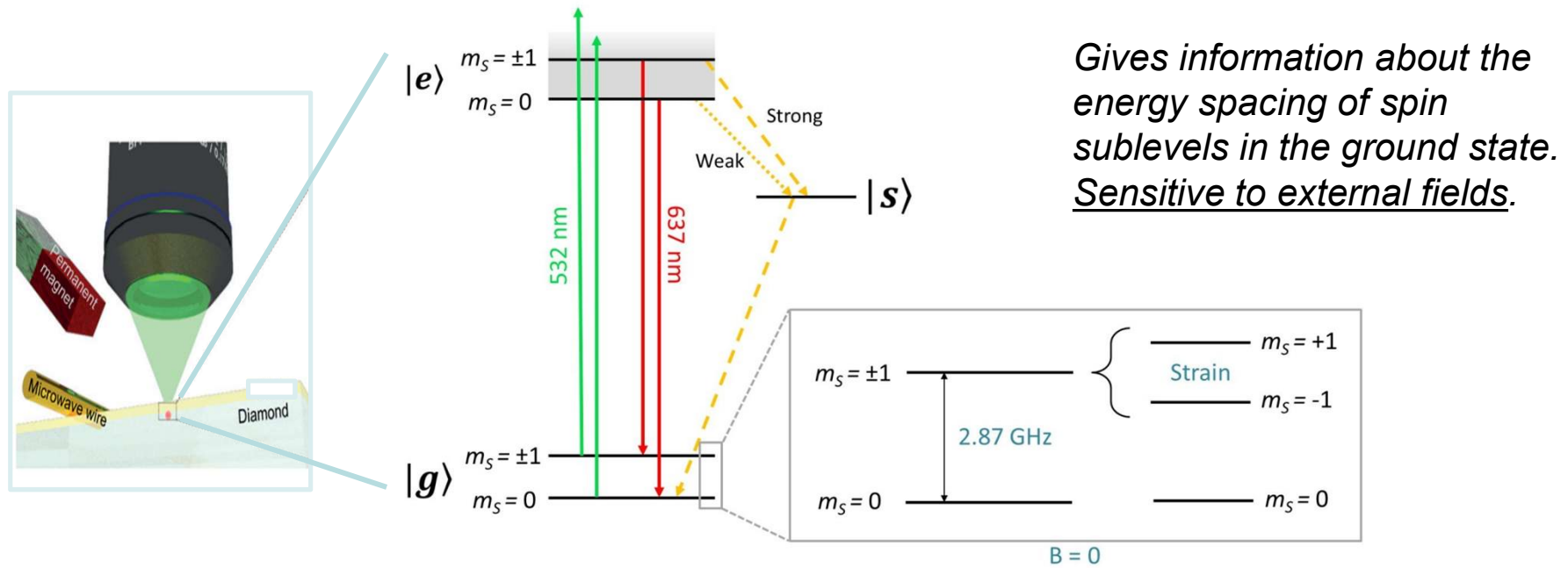
## Spin dynamics in the N-V- center on diamond:

Excitation with green light places the NV in the triplet excited state. Relaxation then emits either a red or (undetected) infrared photon, placing the centre in the  $m_s = 0$ . Microwave pumping raises the centre to  $m_s = \pm 1$ , where Zeeman splitting can occur.

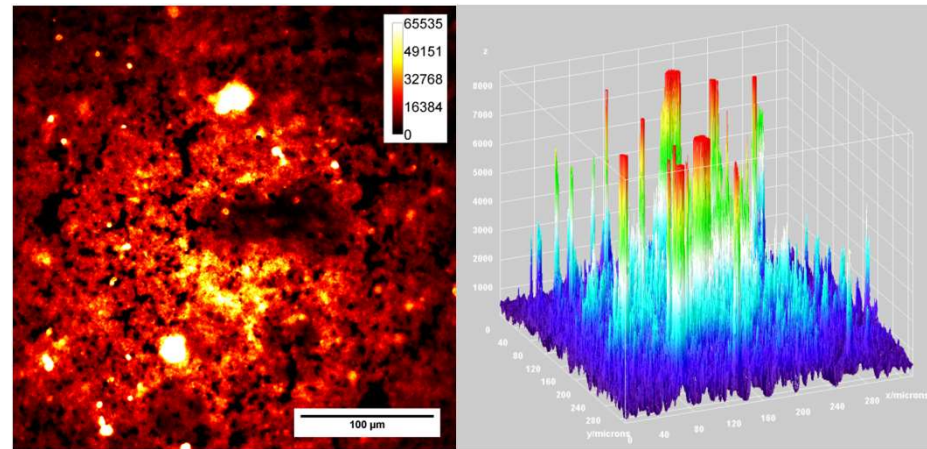
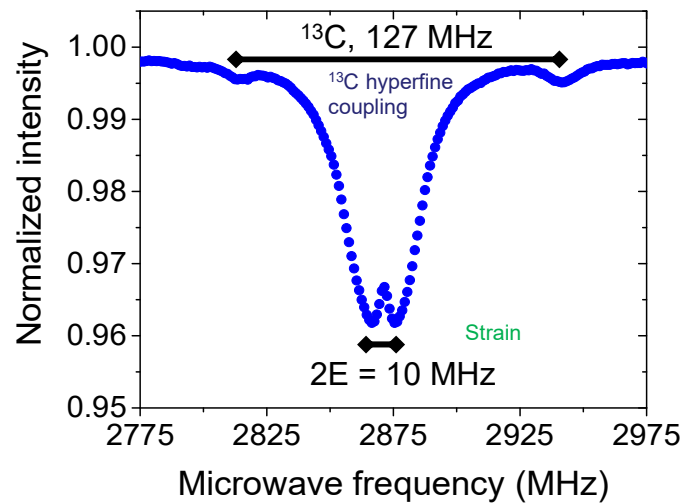
L. Gordon et al.. "Quantum computing with defects". MRS Bulletin. 38 (10): 802–807. doi:10.1557/mrs.2013.206



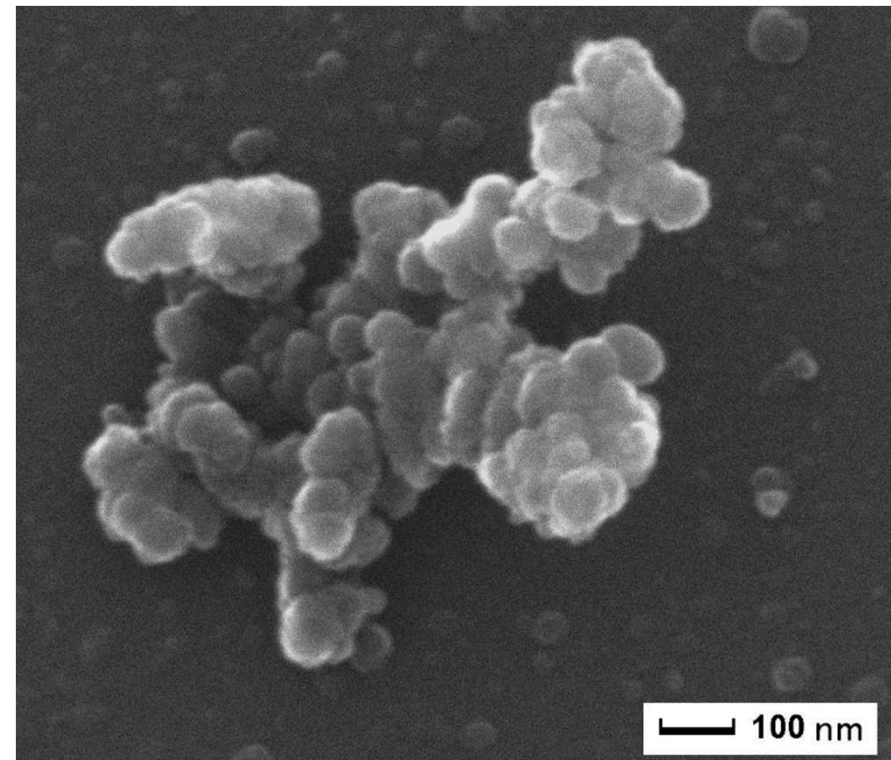
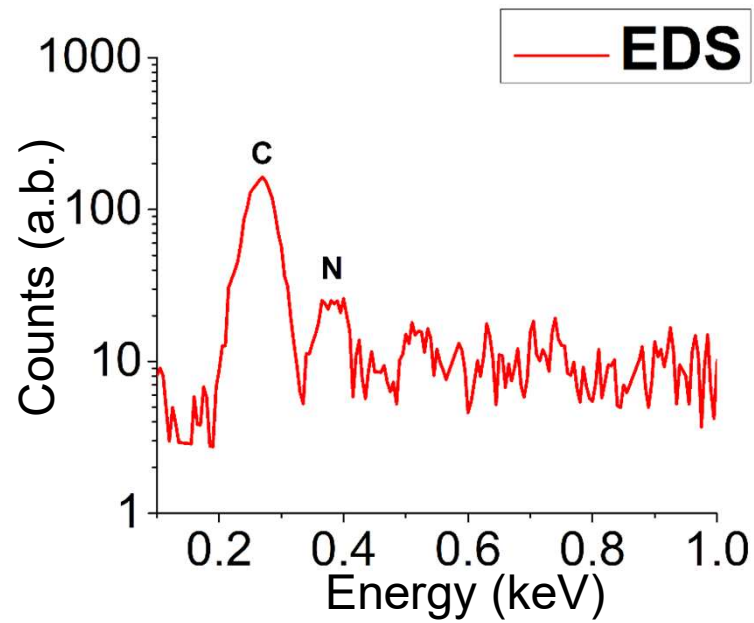
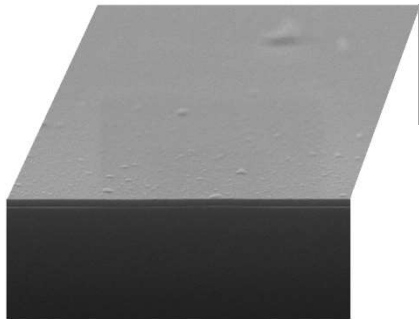
# Optically detected magnetic resonance (ODMR)



*Gives information about the energy spacing of spin sublevels in the ground state. Sensitive to external fields.*

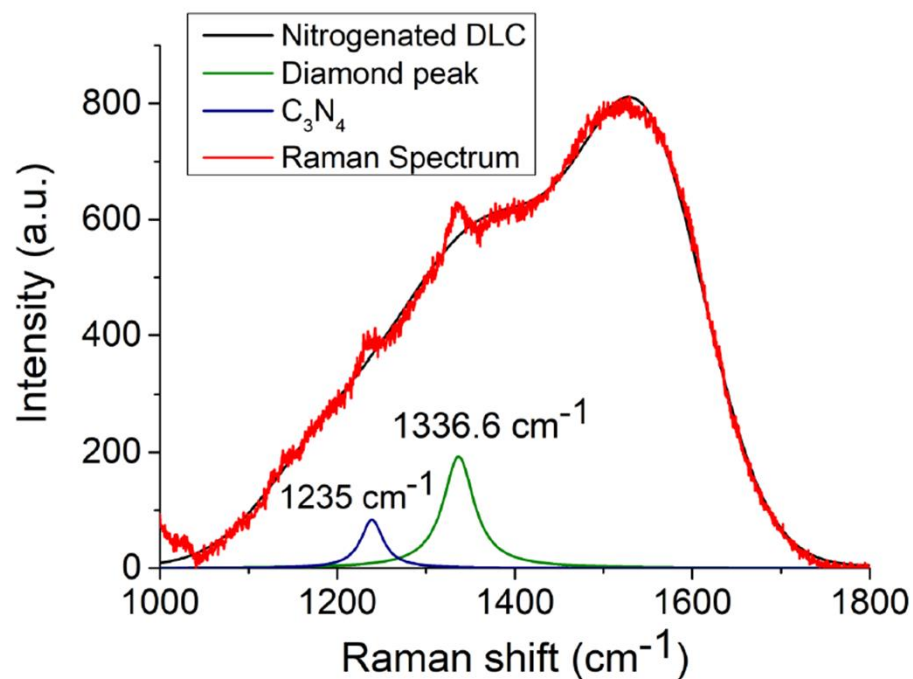


SEM analysis shows clustered **nanoparticles** having dimension  $< 100\text{nm}$

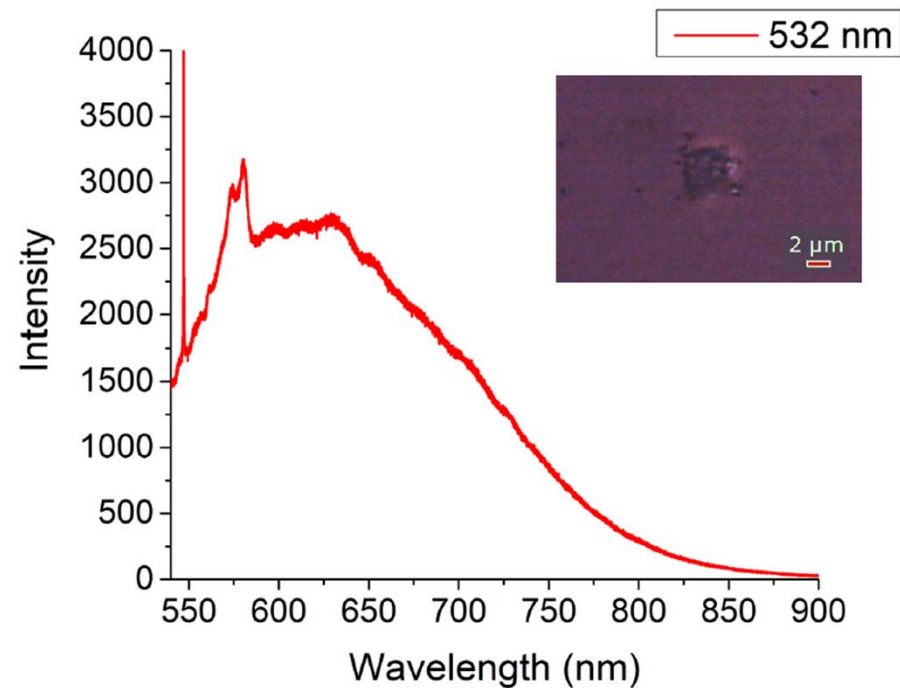


Scanning electron microscopy (**SEM**) image

Energy dispersive X-ray spectroscopy (**EDS**) spectrum



Peak of NDs is **blue-shifted** respect to bulk diamond Raman peak at  $1332 \text{ cm}^{-1}$ , due to compressive-strained nanocrystals.



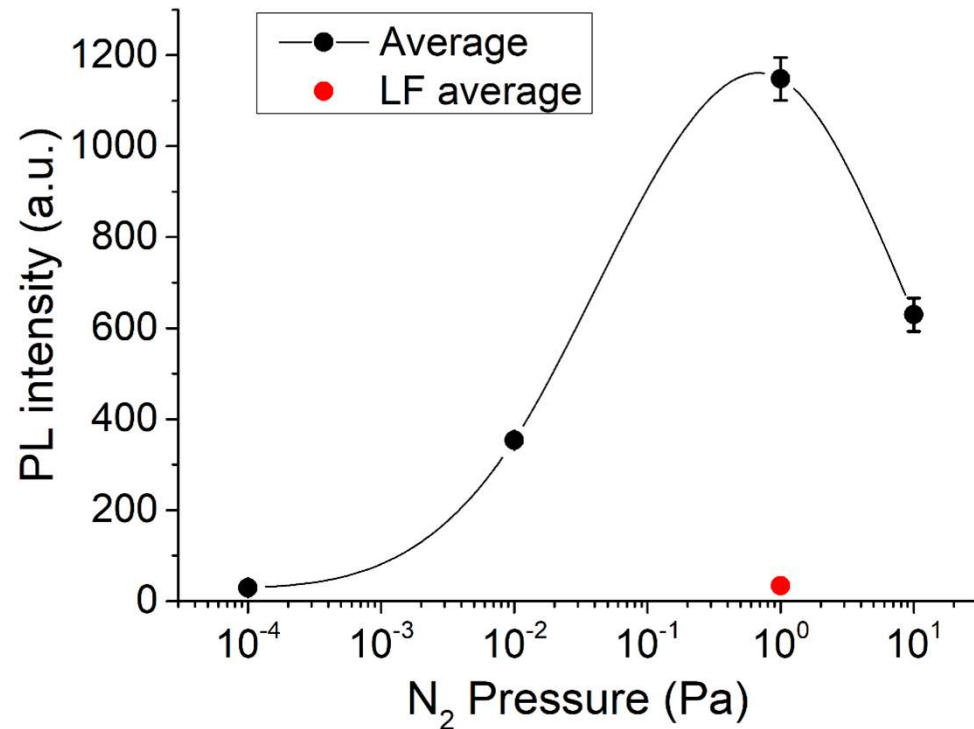
**Photoluminescence (PL)** of deposited clustered nanoparticles: consistent with literature-reported NV emission from NDs enclosed in a graphitic shell.

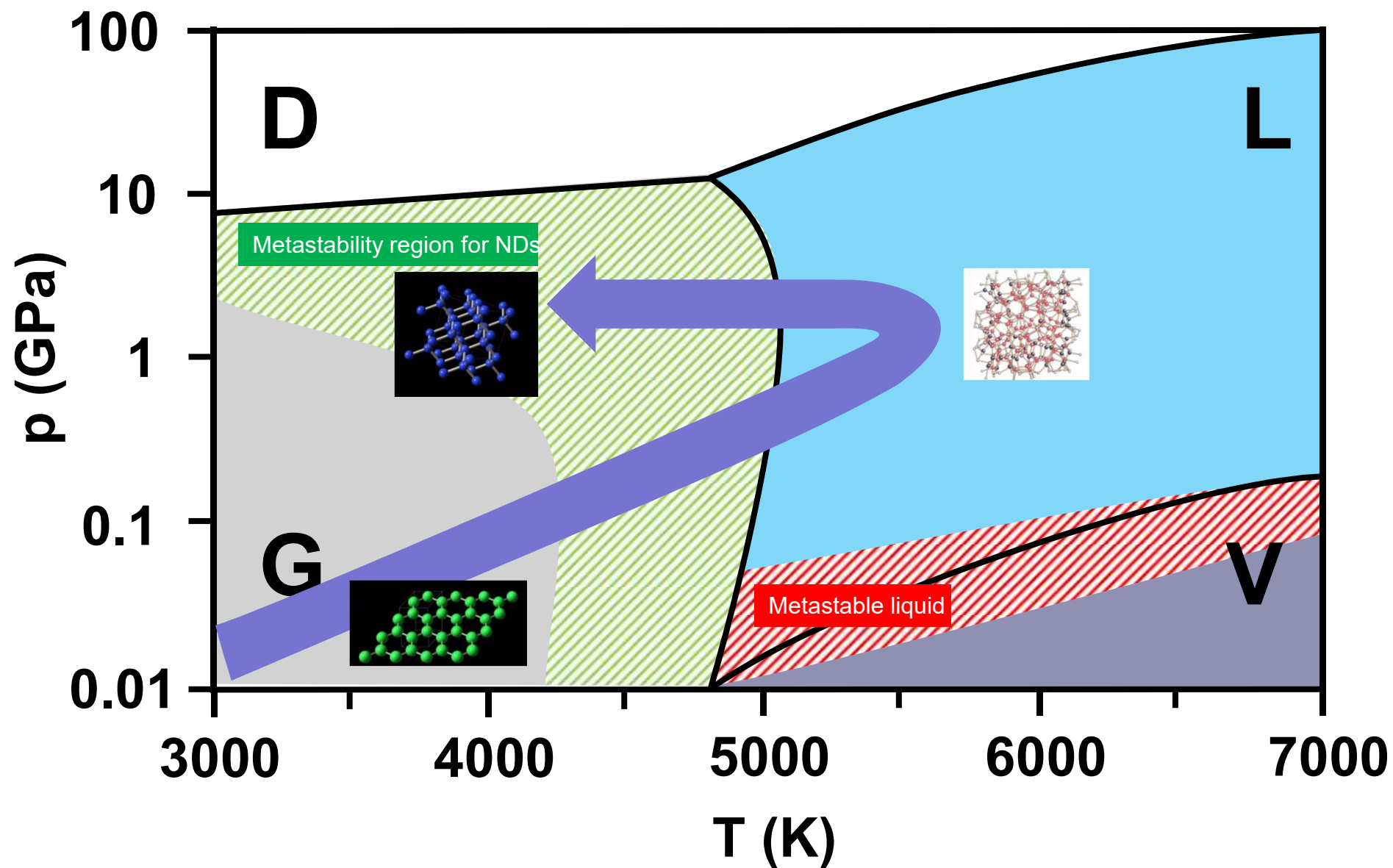
# Thermodynamic model

A **rapid quenching** of liquid carbon is associated with the synthesis of NDs, even at a relatively low pressure. Under these conditions, the Gibbs free energies of liquid carbon and diamond are **equivalent** and the liquid rearranges into a **ND structure**.

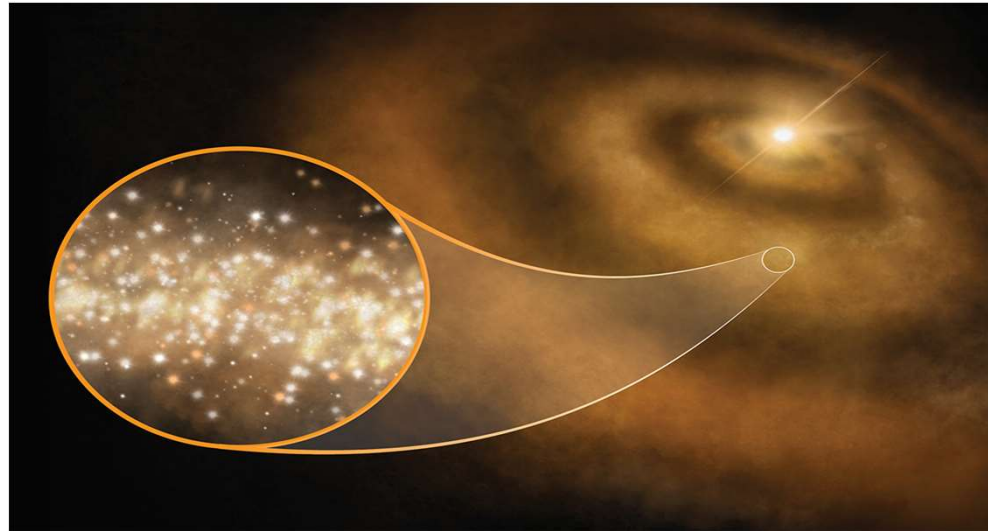
To check this model of NDs formation from liquid to diamond:

Sample prepared with laser fluence of  $1.6 \text{ J cm}^{-2}$ , below threshold for phase explosion of graphite ( $3 \text{ J cm}^{-2}$  [3])





**Nanodiamonds have been identified as the reason for a cosmic glow coming from certain parts of the Milky Way galaxy. The extended red emission (ERE) is a possible manifestation of the NV center in NDs**



**[J. S. Greaves](#) et al. *Anomalous microwave emission from spinning nanodiamonds around stars: Nature Astronomy* (2018) [Published: 11 June 2018](#)**

# Conclusions

- Laser- irradiation of materials permits to **explore thermodynamics in extreme conditions.**

## **Laser- ablation permits to produce:**

- **DLC coatings** having application as optical windows, magnetic storage disks, car parts, biomedical coatings and as micro-electromechanical devices.
- **Nanodiamonds:** quantum-sensing properties of NV-centers in diamonds for nanomagnetometry (also at the nT/ $\mu$ T regime), nanoelectrometry, nanothermometry, detection of strain fields, confocal and fluorescent bioimaging, spin polarization and NMR signal enhancement, quantum optics (proposed as solid-state qubit)